Suleiman-El-Hattab syndrome: a histone modification disorder caused by TASP1 deficiency

Korbinian M Riedhammer, Anna L Burgemeister, Jeanne Amiel, Vincent Cantagrel, Karine Siquier-Pernet, Nathalie Boddaert, Jozef Hertecant, Patricia L Kannouche, Caroline Pouvelle, Stephanie Htun, et al.

Suleiman-El-Hattab syndrome: a histone modification disorder caused by TASP1 deficiency

Korbinian M. Riedhammer [1,2], Anna L. Burgemeister[3], Vincent Cantagrel[4], Jeanne Amiel[5], Karine Siquier[4], Nathalie Boddaert[6], Jozef Hertecant[7], Patricia L. Kannouche[8], Caroline Pouvelle[8], Stephanie Htun[9], Anne M. Slavotinek[9], Christian Beetz[10], Dan Diego-Alvarez[10], Kapil Kampe[10], Nicole Fleischer[11], Zain Awamleh[12], Rosanna Weksberg [12,13,14], Robert Kopajtich[1,15], Thomas Meitinger[1], Jehan Suleiman[16,17] and Ayman W. El-Hattab[18,19,20,*]

[1]Institute of Human Genetics, Klinikum rechts der Isar, School of Medicine, Technical University of Munich, Munich, Germany
[2]Department of Nephrology, Klinikum rechts der Isar, School of Medicine, Technical University of Munich, Munich, Germany
[3]Genetikum, Genetic Counseling and Diagnostics, Stuttgart, Germany
[4]Developmental Brain Disorders Laboratory, Paris University, Imagine Institute, INSERM UMR, Paris, France
[5]Department of Genetics, AP-HP, Necker Enfants Malades Hospital, Paris University, Imagine Institute, Paris, France
[6]Département de radiologie pédiatrique, INSERM UMR 1163 and INSERM U1000, AP-HP, Necker Enfants Malades Hospital, Paris, France
[7]Division of Genetics and Metabolic, Department of Pediatrics, Tawam Hospital, Al Ain, United Arab Emirates
[8]CNRS UMR 9019, Université Paris-Saclay, Equipe labellisée Ligue contre le Cancer, Gustave Roussy, Villejuif, France
[9]Department of Pediatrics, Division of Genetics, University of California, San Francisco, San Francisco, CA, USA
[10]Centogene GmbH, Rostock, Germany
[11]FDNA Inc., Boston, MA, USA
[12]Genetics and Genome Biology, Research Institute, The Hospital for Sick Children, Toronto, Ontario, Canada
[13]Division of Clinical and Metabolic Genetics, The Hospital for Sick Children, Toronto, Ontario, Canada
[14]Institute of Medical Sciences, University of Toronto, Toronto, Ontario, Canada
[15]Institute of Neurogenomics, Helmholtz Zentrum München, Neuherberg, Germany
[16]Division of Neurology, Department of Pediatrics, Tawam Hospital, Al Ain, United Arab Emirates
[17]Department of Pediatrics, College of Medicine and Health Sciences, United Arab Emirates University, Al Ain, United Arab Emirates
[18]Department of Clinical Sciences, College of Medicine, University of Sharjah, Sharjah, United Arab Emirates
[19]Genetics Clinics, University Hospital Sharjah, Sharjah, United Arab Emirates
[20]Genetics and Metabolic Department, KidsHeart Medical Center, Abu Dhabi, AQ6 United Arab Emirates

*To whom correspondence should be addressed at: College of Medicine, University of Sharjah, P.O. Box 27272, Sharjah, United Arab Emirates. Tel: +971 508875123;
Email: elhattabaw@yahoo.com

Abstract

Introduction: *TASP1* encodes an endopeptidase activating histone methyltransferases of the KMT2 family. Homozygous loss-of-function variants in *TASP1* have been associated with Suleiman-El-Hattab syndrome. We report a cohort of 6 individuals with Suleiman-El-Hattab syndrome and provide functional data. **Materials and Methods:** Chromosomal microarray and exome sequencing were performed. Western Blotting from fibroblasts was done for two individuals. RNA sequencing and quantitative proteomics from fibroblasts of one individual were done. Zebrafish *tasp1* knock-out orthologue was created and studied. Methylome analysis in two individuals were performed. **Results:** All individuals had biallelic *TASP1* loss-of-function variants and a neurodevelopmental phenotype including developmental delay, multiple congenital anomalies, distinctive facial appearance, and happy demeanor. Western Blot revealed absence of TASP1 protein. RNA sequencing/proteomics showed *HOX* gene downregulation and dysregulation of the general transcription factor TFIIA. Zebrafish *tasp1* knock-out revealed smaller head size in tasp1 mutants. Methylome analysis showed a distinct methylation profile intermediate between control and Kabuki syndrome (*KMT2D*) profiles. **Discussion:** This work further delineates Suleiman-El-Hattab syndrome, a recognizable neurodevelopmental syndrome. Possible downstream mechanisms of TASP1 deficiency are perturbed HOX gene expression and dysregulated TFIIA complex. Methylation pattern suggests that Suleiman-El-Hattab syndrome can be categorized into the group of histone modification disorders like Wiedemann-Steiner and Kabuki syndrome.

Introduction

Homozygous loss-of-function variants in *TASP1* (MIM *608270) have recently been associated with an autosomal recessive syndrome featuring developmental delay, happy demeanor, distinctive facial features, and congenital anomalies.[1] It has been termed “Suleiman-El-Hattab syndrome” (MIM #618950).

TASP1 encodes taspase 1 (threonine aspartase 1, TASP1). This enzyme functions as an endopeptidase activating various nuclear factors, including histone methyltransferases of the evolutionary conserved KMT2 family of proteins like KMT2A and KMT2B, which are part of the epigenetic machinery.[2] Epigenetic marks are modifications of DNA (e.g., methylation of cytosine nucleotides) or histone tails influencing transcriptional activity of genes without altering the DNA sequence itself.[3] Due to this central role in regulation of transcriptional activity, it is not surprising that variation in genes of the epigenetic machinery can result in Mendelian disorders. Haploinsufficiency of *KMT2A* has been associated with Wiedemann-Steiner syndrome (MIM #605130).[4] Haploinsufficiency of *KMT2B* has been associated with complex childhood-onset dystonia (MIM #617284).[5] Another member of the evolutionary conserved KMT2 family of histone methyltransferases is *KMT2D*. Haploinsufficiency of *KMT2D* has been associated with Kabuki syndrome 1 (MIM #147920).[6]

To date, Suleiman-El-Hattab syndrome has been described in 4 individuals. We here present 6 individuals with Suleiman-El-Hattab syndrome including three previously unreported individuals and three previously reported individuals with updated phenotypic information. We further delineate the phenotypic and genotypic spectrum of this newly described syndrome, and additionally present both *in vitro* and *in vivo* functional work showing the consequences of biallelic *TASP1* loss-of-function variants.

Materials and Methods

Recruitment of individuals

Individuals were seen in pediatric neurology and/or genetics departments of the respective institutions. Some of the individuals have been connected via GeneMatcher.[7] Written informed consent for sequencing and publication in a scientific journal (including photographs) was obtained by the legal guardians according to the Declaration of Helsinki and the study has been approved by the ethical committee of the respective institutions.

Molecular genetic testing

Chromosomal microarray (CMA) for individual 1 was performed at Baylor Genetics Laboratory, Houston, Texas, USA, as previously described.[8] CMA for individual 2 was performed at Tawam Hospital Genetics Laboratory, Al Ain, United Arab Emirates using CytoScan™ HD Array as per the manufacturer's instructions. CMA for individual 3 was performed at Centogene AG, Rostock, Germany, using CentoArrayCyto™. Breakpoint mapping in for this individual was performed using gene specific primers (F: 5' AAGGCACTCGCAAGTAACTG 3'; R: 5' CACTGGAAAGACAGCTTGATGC 3') to amplify the deleted allele.[1] PCR product was later sequenced on a 3730xl capillary sequencer (Applied Biosystems) to identify the breakpoints. CMA for individual 4 was performed at PreventionGenetics, Marshfield, Wisconsin, USA, as previously described.[9] Exome sequencing for individual 5 was performed at Helmholtz Zentrum München, Neuherberg, Germany, as previously described.[10,11] Sanger sequencing was

used to test the individual's parents. Trio exome sequencing for individual 6 and parents was done at Imagine Institute, Paris, France, as previously described.[12]

Distinct facial gestalt

To establish a reproducible facial gestalt for Suleiman-El-Hattab syndrome, the facial recognition software DeepGestalt was used.[13] The analysis of images was first pre-processed to achieve facial detection, landmark detection and alignment. After preprocessing, the input image was cropped into facial regions. Each region was fed into a Deep Convolutional Neural Network (DCNN) to obtain a softmax vector indicating its correspondence to each syndrome in the model. The analysis of visual facial data was used to form a mathematical representation of the face (facial descriptor) which can be readily compared to other such descriptors (i.e. facial gestalt of other syndromes). To enable visualization of these vectors, a composite image was produced.

Western Blot

Primary fibroblasts 405VI wt (wild type) from a healthy donor, primary fibroblasts TASP1-Arg67* (individual 5), primary fibroblasts TASP1-trunc (individual 6), and tumor cells HeLa (ATCC CCL-2) were cultivated in D-MEM containing 100 U/ml penicillin, 100 µg/ml streptomycin and 10% fetal calf serum (FCS). All cell lines were incubated at 37°C in an atmosphere containing 5% CO_2 and were regularly tested for mycoplasma. siRNAs were purchased from Horizon discovery : *hTASP1* (L-004745-00-0005) and non-targeting siRNA (NT, D-001810-01-05) were used as control. Cells were transfected with 30nM of siRNAs using Interferin (Polyplus) according to the manufacturer's instructions and were processed 72 hours later. Protein extracts were prepared and processed for

SDS-PAGE as previously described.[14] Membranes were then blotted with indicated antibodies: rabbit polyclonal TASP1α (Proteintech 16739-1-AP, 1:500) and mouse IgG1 β-catenin (BD biosciences clone 14, 1:2000).

RNA sequencing and proteomics

RNA sequencing of individual 5 was performed as strand-specific mRNA according to the TruSeq Stranded mRNA Sample Prep Guide on a NovaSeq 6000 platform (Illumina) at Helmholtz Zentrum München, Neuherberg, Germany, as previously described.[11] In order to detect differentially expressed genes, RNA sequencing data of individual 5 was analyzed using the method OUTRIDER in a cohort of 269 control samples.[15]

Quantitative tandem mass tag (TMT) proteomics was performed at the BayBioMS core facility at the Technical University Munich, Freising, Germany, and is described in detail on medRxiv (https://www.medrxiv.org/content/10.1101/2021.03.09.21253187v2.full, in revision).

DNA methylation pattern

Genomic DNA extracted from blood was treated with sodium bisulfite using the EpiTect PLUS Bisulfite Kit (QIAGEN) and hybridized to the Illumina Infinium Human Methylation EPIC BeadChip to interrogate more than 850,000 CpG sites at The Center for Applied Genomics (TCAG), Hospital for Sick Children Research Institute, Toronto, Canada. The *TASP1* samples with age-and sex-matched typically developing controls were run in two batches. The minfi Bioconductor package was used to preprocess data including quality control, Illumina normalization and background subtraction, and

extraction of β values. Probes with detection flaws, probes near single-nucleotide polymorphisms (SNPs) with minor allele frequencies above 1%, cross-reactive probes, probes with raw beta of 0 or 1 in > 0.25% of samples, non-CpG probes, and sex chromosome probes were removed according to our published pipeline.[16] A total of *n* = 774,558 probes remained for interrogating DNA methylation (DNAm) levels. *TASP1* samples (DNA of individuals 3 and 5) were compared to DNAm data from typically developing controls (*n* = 65) and individuals clinically diagnosed with Kabuki Syndrome 1 with a pathogenic *KMT2D* variant (*n* = 5).[17]

Zebrafish

All animal experiments were performed under a protocol approved by the Institute for Animal Care and Use Committee. A Clustered Regularly Interspaced Short Palindromic Repeats (CRISPR) small guide (sg)RNA targeting exon 5 of *tasp1* (ENSDART00000133661.3) was designed. sgRNA and Cas9 protein were co-injected into wildtype EKW zebrafish eggs and F0 founders with small indels in *tasp1* at the target site were selected. Adult F1 heterozygotes with germline *tasp1* indel variants were crossed to obtain F2, homozygous larvae. Larvae were cryosectioned and hematoxylin and eosin staining was performed. For measurements of brain size, 12 µm sections through the optic nerve of both eyes from *tasp1* indel homozygotes and wildtype larvae were selected and an average of five consecutive sections containing the diencephalon were measured using Image J software; measurements were averaged for 3 larvae from each group. Alcian blue staining was performed according to prior methods.[18]

Results

Phenotypic characteristics

We present 6 individuals from 5 unrelated families with Suleiman-El-Hattab syndrome with biallelic putative loss-of-function variants in *TASP1* (Table 1 and Figure 1). Individual 1 was a seven-year-old boy with global developmental delay (walked at age three years, can say only 2 simple words from age three years on), hypotonia, microcephaly, feeding difficulties, salivary drooling, failure to thrive, recurrent respiratory infections, cryptorchidism, cardiovascular malformations (atrial septal defect [ASD] and ventricular septal defect [VSD]), moderate mixed-type hearing impairment in right ear, limb deformities (clinodactyly, left single palmer crease, brachydactyly), hirsutism, a happy demeanor with frequent laughing and clapping, and distinctive facial features (Figure 1A and 1C). This individual was previously reported in Suleiman, et al., 2019, as case 1.[1]

Individual 2, the younger brother of individual 1, was a nine-months-old boy with global developmental delay (poor head control, inability to roll, and only making babbling sounds), hypotonia, macrocephaly, cardiovascular malformations (tetralogy of Fallot [TOF]), feeding difficulties, failure to thrive, preauricular skin tag, overlapping toes, lumbar skin dimple, and distinctive dysmorphic features (Figure 1B and 1C). Cranial MRI at the age of eight months showed cystic dilatation of the fourth ventricle, with massively enlarged posterior fossa and hypoplasia/agenesis of the cerebellar vermis (consistent with severe form of Dandy-walker malformation; DWM) and hydrocephalus (Figure 2A). Ventriculoperitoneal shunt and fenestration of posterior fossa cyst were performed at age nine months.

Individual 3 was a 19-month-old girl with global developmental delay (cruised around furniture at age 18 months, babbling sounds at 10 months of age), hypotonia, microcephaly, cardiovascular malformation (PFO and VSD), feeding difficulties, salivary drooling, failure to thrive, hirsutism, umbilical hernia, sacral hair tuft, webbed neck, happy demeanor, and distinctive dysmorphic features (Figure 1D). Cranial MRI at age five months showed a small right cerebellopontine angle cyst and hypoplasia of the splenium of corpus callosum (Figure 2B). Spine MRI revealed diffuse dural ectasia of the lower dorsal and lumbar spinal canal.

Individual 4 was a three-year-old girl with global developmental delay (walked at age 2.5 years, remains non-verbal), hypotonia, microcephaly, feeding difficulties, salivary drooling, failure to thrive, recurrent respiratory infections, cardiovascular malformations (patent foramen ovale [PFO] and VSD), left hydronephrosis, bilateral hyperopia, hirsutism, preauricular skin tag, polydactyly, bilateral single palmar creases, congenital dermal melanosis, happy demeanor with frequent laughing, and distinctive dysmorphic features (Figure 1E and 1F). Cranial MRI at three months of age showed widening of the extra-axial CSF spaces and sulci bifrontally, suggestive of benign enlargement of the subarachnoid spaces in infancy (BESS). This case was previously described in Suleiman et al., 2019, as case 2.[1]

Individual 5 was a six-year-old boy with global developmental delay (walked at age 3 years, remains non-verbal), hypotonia, microcephaly, feeding difficulties, seizures, recurrent respiratory infections, VSD, cryptorchidism, inguinal hernias, pale optic disks, convergent strabismus, amblyopia of left eye, a periauricular skin tag on the left tragus, bilateral single palmar creases, happy demeanor, and distinctive facial features (Figure 1G and 1H). Cranial MRI at the age of two years and five months revealed malformation

of posterior fossa (dilatation of the fourth ventricle that directly communicate with mildly enlarged posterior fossa, with associated hypoplastic inferior cerebellar vermis), dilatation of lateral and third ventricles, and periventricular white matter hyperintensity around posterior horn of lateral ventricle bilaterally (Figure 2C). This case was previously described in Suleiman et al., 2019, as case 4.[1]

Individual 6 was a ten-year-old girl with global developmental delay (walked at age 21 months, had only few single words), lower limb spasticity, microcephaly, feeding difficulties, VSD, anteriorly placed anus that was corrected surgically, chronic nasal obstruction with choanal stenosis, hirsutism, limb deformities (short extremities, brachydactyly, hypoplastic terminal phalanges, and broad thumbs and first toes), scoliosis, genu recurvatum, hyperopia, and distinctive facial features (Figure 1I and 1J). Cranial MRI at age 6 years showed malformation of posterior fossa (dilatation of the fourth ventricle that directly communicate with a retrocerebellar cyst, with associated hypoplastic inferior cerebellar vermis), as well as dilatation of lateral and third ventricles. (Figure 2D). She had had a sister with bilateral choanal atresia, anteriorly placed anus, and a retrocerebellar cyst, who died at age of 6 months before performing any genetic tests.

DeepGestalt software could establish a distinct facial gestalt for Suleiman-El-Hattab syndrome (Figure 1K). The descriptor of photos of individuals genetically diagnosed with Suleiman-El-Hattab syndrome is distinct from all other descriptors of syndromes in the dataset (300+) achieving an area under the curve (AUC) of 0.975 (95% confidence interval 88 – 93%).

Genotypic characteristics

CMA in individual 1 revealed a homozygous deletion at 20p12.1 with a minimum deletion boundary of chr20:g.13,463,860 – 13,532,560 (hg19). This deletion encompasses part of *TASP1* (NM_017714.3). Breakpoint mapping revealed that this deletion is 149.4 kb in size spanning chr20:g.13,448,380-13,597,783 and includes exons 5 – 11 of *TASP1*.[1] CMA in individual 2, brother of individual 1, also revealed the same deletion in a homozygous state. CMA in individual 3 revealed a homozygous deletion at 20p21.2 with a minimum deletion boundary of ch20:g.13,447,411 – 13,606,048. Breakpoint mapping revealed the same boundaries in individual 1 (chr20:g.13,448,380-13,597,783), including exons 5 – 11 of *TASP1*. CMA in individual 4 identified a homozygous deletion with a minimum deletion boundary of chr20:g.13,466,774 – 13,593,390. Breakpoint mapping revealed the same boundaries in individual 1 (chr20:g.13,448,380 – 13,597,783), including exons 5 – 11 of *TASP1*.[1] For these individuals, parents were found to be heterozygous for the deletion, and none of the healthy siblings were found to have a homozygous deletion in this region (Figure 1C, 1D, and 1F). This intragenic deletion disrupts the active site of the enzyme (at amino acid position 234; NP_060184.2; see https://www.uniprot.org/uniprot/Q9H6P5/protvista) and is predicted to lead to a frameshift supporting the loss-of-function nature of this variant.[1,19]

Exome sequencing in individual 5 revealed a homozygous nonsense variant in *TASP1* c.199C>T, p.(Arg67*) (chr20:g.13,605,846G>A). The variant p.Arg67* was reported once in a heterozygous state in the Genome Aggregation Database (gnomAD v.2.1.1, https://gnomad.broadinstitute.org/; allele frequency of 4×10^{-6}) indicating that it is an extremely rare variant. This variant is predicted to either lead to nonsense-

mediated decay or a truncated protein leading to a complete loss of function. Both parents are confirmed to be heterozygous carriers for this variant (Figure 1H). Trio exome sequencing in individual 6 revealed compound-heterozygous frameshift variants c.81del, p.(Glu29Serfs*79) (chr20:g.13,610,645del) and c.598_599del, p.(Lys200Glufs*24) (chr20:g.13,539,731_13,539,732del). The father is heterozygous carrier of the p.Glu29Serfs*79 variant and the mother is heterozygous carrier of the p.Lys200Glufs*24 variant (Figure 1J). Both variants have not been listed in over 140,000 individuals in gnomAD. Both variants are predicted to either leading to nonsense-mediated decay or a truncated protein. Figure 1L summarizes the localization of the different *TASP1* pathogenic variants within the gene and protein.

Western Blot

Western Blot from primary fibroblasts from individuals 5 and 6 confirmed that TASP1 protein (cleaved form p28) is not observed in these cells compared to primary fibroblasts from healthy donor (Figure 1M). The specificity of the TASP1 antibody was verified by downregulating *TASP1* gene expression using specific siRNAs. A clear reduction of TASP1 protein levels with transfection in HeLa cells was observed (Figure 1N).

RNA sequencing and proteomics

RNA sequencing from fibroblasts of individual 5 revealed 20 significant differentially expressed genes (Supplementary Table S1). Notable differentially expressed genes were: *GTF2A1* (adjusted $p = 8.15 \cdot 10^{-7}$), which was upregulated (log2fc = 0.55); *HOXA4* (adjusted $p = 5.02 \cdot 10^{-4}$; log2fc = -5.42), *HOXA7* (adjusted $p = 7.86 \cdot 10^{-4}$;

log2fc = -5.4), *HOXB2* (adjusted $p = 9.5 \cdot 10^{-3}$; log2fc = -1.8) and *HOXA1* (adjusted p = 0.0312, log2fc = 5.15), which were all downregulated (Figure 3A).

Quantitative proteomics from fibroblasts of individual 5 resulted in the identification of 13 significant aberrant protein levels (Supplementary Table S2). One notable significant outlier was GTF2A2 (adjusted p = 0.001770059; log2fc = 1.74), which was upregulated (Figure 3B). TASP1 protein was not detected in the corresponding TMT-batch, hence proteomics was not able to provide any additional evidence on TASP1 protein stability.

DNA methylation pattern

Since the number of available *TASP1* samples is not sufficient to establish a robust disorder-specific signature, we clustered the DNAm profiles of two individuals carrying homozygous loss-of-function *TASP1* variants, individual 4 (deletion exons 5 – 11) and individual 5 (p.Arg67*), using the published Kabuki syndrome 1 signature.[17] Principal component analysis (PCA) based on DNAm values at 114 Kabuki syndrome 1 signature sites clearly distinguishes the DNAm profile of healthy controls from DNAm profiles of the five individuals with Kabuki syndrome 1 on the first principal component (PC1) and the two individuals carrying *TASP1* variants on PC2 (Figure 3C). Hierarchal clustering shows that, at Kabuki syndrome 1 signature sites, individuals carrying *TASP1* variants have distinct DNAm profiles that are intermediate when compared to the DNAm profiles of Kabuki syndrome 1 individuals and controls (Figure 3D).

Zebrafish experiments

We were successfully able to target the single, *tasp1* gene in *Danio rerio* and generate homozygous, F2 larvae with an indel variant predicting a loss of function, *tasp1* c.313_314delTC, p.Ser105Gly*fs**2 (ENSDART00000133661.3; Figure 4A). Sectioning and staining of larval heads at 6 dpf showed wildtype EKW had an average brain area of 15,596 μm2 (Figure 4B) compared to 14,747 μm2 in larvae homozygous for the *tasp1* indel variant (Figure 4C). A comparison of the cranial cartilages stained with Alcian blue in wildtype larvae (Figure 4D) and homozygous, *tasp1* indel larvae (Figures 4G and J) showed that *tasp1* crispant larvae had smaller trabeculae and shorter ethmoid cartilages compared to wildtype larvae. Wildtype larvae also had longer ceratobranchial and ceratohyal cartilages (Figure 4E) compared to homozygous, *tasp1* indel larvae (Figures 4H and K). Wildtype larvae had longer lower jaw lengths and larger palatoquadrate and Meckel's cartilages (Figure 4F) compared to homozygous, *tasp1* indel larvae (Figures 4I and L).

Discussion

We here report phenotypic, genotypic, and functional data on the largest cohort of individuals with the recently characterized Suleiman-El-Hattab syndrome caused by biallelic loss-of-function variants in *TASP1*. The cohort presented here features 6 individuals with Suleiman-El-Hattab syndrome. Also included in the discussion and Table 1 is a seventh individual, previously described as case 3 in Suleiman et al., 2019.[1]

These 7 individuals have an overlapping phenotype of global developmental delay (7/7) with delayed motor development and severe speech delay (4/7 non-verbal at ages 3 – 10 years), microcephaly (6/7) and brain malformations (6/7), hypotonia (6/7),

feeding difficulties (6/7), a happy demeanor (5/7) and congenital anomalies like cardiovascular malformations (6/7), which were mostly mild (ASD/VSD with spontaneous resolution), however; one individual had severe cardiac malformations (TOF) and required surgery (Table 1).

Notably, concerning brain malformations, 4/6 individuals had cystic malformations of the posterior fossa, with variable degrees including small cerebellopontine angle arachnoid cyst, dilated 4th ventricle with enlarged posterior fossa along with cerebellar vermian hypoplasia, to the full extent of classic Dandy Walker malformation associated with hydrocephalus (individuals 2, 3, 5 and 6; Figure 2).[20,21] This extends the neurologic phenotype of Suleiman-El-Hattab syndrome and might further help neurologists and radiologists in recognition of this syndrome. In addition, this supports the notion that imaging findings of cerebellar hypoplasia and Dandy Walker malformation are often associated with underlying genetic causes and should prompt further evaluation.[22]

Affected individuals feature a distinctive facial pattern, as also mathematically proven by DeepGestalt software, involving thick and arched eyebrows with synophrys, epicanthus, downslanted palpebral fissures, hypertelorism, broad nasal bridge, long and smooth philtrum, wide mouth with thin upper lip and thick lower lip, microretrognathia and ear anomalies (dysplastic, low-set).[13] This makes the syndrome recognizable by clinical geneticists and the syndrome is now featured in the Face2Gene online tool (FDNA Inc., USA).

TASP1 encodes the proenzyme taspase 1 (threonine aspartase 1, TASP1), which is cleaved into two subunits, alpha and beta, in an autocatalytic fashion, which in turn form the active heterodimeric enzyme, an endopetidase. The active enzyme uses the N-terminal threonine at amino acid position 234 (p.Thr234) of the mature beta subunit as

the active-site nucleophile to proteolyze polypeptide substrates. This endopeptidase cleaves various nuclear factors after an aspartate, hence it is called threonine aspartase (taspase). For example, active TASP1 cleaves and hence activates histone methyltransferases of the KMT2 protein family like *KMT2A* and *KMT2B*. Cleavage of *KMT2A* (also known as *MLL1*) in turn is crucial for *HOX* and cyclin gene expression which is important for cell cycle dynamics.[2,23] In line with this, individual 5, who harbors a homozygous nonsense variant in *TASP1* and has no detectable TASP1 protein on Western Blot (Figure 1M), showed significant RNA downregulation of HOX genes *HOXA4*, *HOXA7, HOXA1* and *HOXB2* (Figure 3A). Coordinated *HOX* expression is central for a correct segmental body plan.[24] Hence, dysregulation of *HOX* genes could play a role in the congenital and neurodevelopmental anomalies observed in TASP1-deficient individuals.

Another substrate of TASP1 is transcription factor TFIIAα−β (*GTF2A1*), a general transcription factor with ubiquitous expression featuring an alpha and beta subunit. TFIIAα−β is bound to TFIIAγ (*GTF2A2*). When TASP1 cleaves the alpha and beta subunit of TFIIAα−β, the heterotrimeric complex TFIIAα/β/γ (encoded by *GTF2A1* and *GTF2A2,* summarized as TFIIA) is susceptible to degradation by the proteasome impeding its transcriptional activity.[2,25] Regulated turnover of TFIIA is key for correct embryonal cell proliferation and morphogenesis. Tasp1-deficient and Tfiia-noncleavable mice both show craniofacial anomalies like jaw, eye and brain malformations.[19] Intriguingly, on RNA sequencing of TASP1-deficient individual 5, *GTF2A1* (TFIIAα−β) is upregulated; and on proteomics, GTF2A2 (TFIIAγ) is upregulated, probably illustrating the stable non-cleaved TFIIA complex (Figures 3A and B). Hence, the neurodevelopmental phenotype in all individuals including the central nervous system

anomalies in Suleiman-El-Hattab syndrome could be due to TFIIA dysregulation including a positive feedback loop (*GTF2A1* upregulation on RNA sequencing).

As TASP1 cleaves and hence activates histone methyltransferases of the KMT2 protein family, it is expected that defects in KMT2 genes result in syndromes with overlapping features of Suleiman-El-Hattab syndrome. Haploinsufficiency of *KMT2A* causes a phenotypically similar disorder, Wiedemann-Steiner syndrome (MIM #605130), also featuring developmental delay, facial dysmorphies, alongside hyptrichosis cubiti, growth failure, skeletal malformations, cardiac anomalies, and microcephaly.[4] Also individuals with haploinsufficiency of *KMT2B* (MIM #617284) can have, additionally to childhood-onset dystonia, facial dysmorphies like elongated face, a bulbous nasal tip, and microcephaly.[26] Haploinsufficiency of *KMT2D* causes Kabuki syndrome 1 (MIM #147920) which is characterized by developmental delay, distinctive facial features, hirsutism, skeletal anomalies, persistence of fetal fingertip pads, recurrent infections, growth failure, seizures, and multiple congenital anomalies.[6]

Intriguingly, Kabuki syndrome 1, Wiedemann-Steiner syndrome, and Suleiman-El-Hattab syndrome share remarkable phenotypic overlap. All three are syndromal intellectual disability/developmental delay syndromes featuring a distinct facial gestalt with thick and arched eyebrows, hirsutism, growth failure, and multiple congenital anomalies. *KMT2A*, *KMT2B*, and *KMT2D* are all part of the highly conserved COMPASS family of histone methyltransferases. The members of the COMPASS protein family catalyze histone H3 lysine 4 (H3K4) methylation and are crucial for regulation of gene expression.[2,27] Hence, our data suggests that Suleiman-El-Hattab syndrome can be grouped into the category of histone modification disorders.

As the *KMT2*-genes encode histone methyltransferases, we sought to investigate the effect of TASP1 deficiency on global methylation pattern. Alterations of the epigenetic machinery can results in distinctive and reproducible methylome DNAm patterns ("episignatures"), as has recently been shown for 34 monogenic neurodevelopmental disorders, including Wiedemann-Steiner syndrome (*KMT2A*). A major advantage of this approach is that episignatures, which can be established by methylome analysis from peripheral blood, can serve as "biomarkers" to classify variants of unknown significance in the respective genes.[28] Due to the small number of investigated individuals, we could not establish a specific methylation pattern for Suleiman-El-Hattab syndrome but, interestingly, could show that the examined cases' (individuals 4 and 5) have a distinct DNAm profile intermediate between Kabuki syndrome 1 and control profiles (Figures 3C and D).

We can also corroborate the effects of *TASP1* loss-of-function by *in vivo* data. Already in 2006, knock-out mouse experiments revealed that *Tasp1*-deficient mice were smaller in size than their wild type counterparts and cell proliferation was reduced in mutant mice.[24] Indeed, also in the 7 individuals with Suleiman-El-Hattab syndrome, feeding difficulties and/or failure to thrive was a common finding (6/7 had feeding difficulties, 5/7 failure to thrive). Microcephaly was also reported in 6 of 7 individuals. Now, by knock-out of *tasp1* orthologue in Zebrafish, we could recapitulate this phenotype as *tasp1* mutants had a smaller head size in comparison to wild type animals (Figures 4B and C). Furthermore, *tasp1* mutants showed abnormal cranial cartilage formation (Figures 4D to L). In line with this finding, individuals with Suleiman-El-Hattab syndrome feature facial anomalies like a broad nasal bridge, wide mouth and microretrognathia (Figure 1K). TASP1 activates KMT2A, and it is interesting to note that

zebrafish injected with antisense morpholinos targeting *kmt2a* have also had significant craniofacial defects, including severe hypoplasia of the cartilaginous structures of the viscerocranium, including complete loss of branchial arches 3–7, Meckel′s cartilage and the ceratohyal cartilages.[29] Moreover, *Tasp1* knock-out mice featured skeletal anomalies (vertebra, ribs, sternum).[24] In our cohort, major skeletal anomalies or dysplasia were not reported but, interestingly, there were three individuals with digital deformities (individuals 1, 4 and 6). Individual 6 also had shortened extremities.

In conclusion, we further delineate the phenotypic and genotypic basis of Suleiman-El-Hattab syndrome by presenting the largest cohort of affected individuals of this recognizable syndrome. In addition, we also provide functional insight in the pathophysiology of Suleiman-El-Hattab syndrome by suggesting the perturbation of *HOX* gene expression and TFIIA complex dysregulation as a possible downstream mechanism of TASP1 deficiency. Furthermore, by methylation pattern analysis, we could show that Suleiman-El-Hattab syndrome can be categorized into the group of histone modification disorders like Wiedemann-Steiner syndrome and Kabuki syndrome.

Figure legends

Figure 1. Pedigrees and photographs of affected individual, Western blot results, and schematic image of *TASP1* gene and corresponding protein. Circles, female individual; crossed circle, deceased female individual; dot within circles/squares, heterozygous carrier of the respective *TASP1* variant; double horizontal line, consanguineous couple; squares, male individual.

A) Individual 1 at seven years of age showing prominent glabella, excessive forehead hair, thick and arched eyebrows with synophrys, epicanthus, hypertelorism, periorbital fullness with thick eyelids, broad nasal bridge, long and smooth philtrum, wide mouth, thin upper lip, thick lower lip, low-set dysplastic ears, and webbed neck.

B) Individual 2 at six months of age showing prominent glabella, thick and arched eyebrows with synophrys, epicanthus, hyperterorism, periorbital fullness with thick eyelids, broad and flat nasal bridge, long and smooth philtrum, wide mouth, thin upper lip, thick lower lip, microretrognathia, low set dysplastic ears, and preauricular skin tag.

C) Pedigree of individuals 1 and 2.

D) Pedigree of individual 3. Parents elected not to publish the individual's photographs. Facial features include prominent glabella, excessive forehead hair, arched and thick eyebrows with synophrys, epicanthus, downslanted palpebral fissures, hypertelorism, periorbital fullness with thick eyelids, broad nasal bridge, long and smooth philtrum, wide mouth, thin upper lip, thick lower lip, microretrognathia, high arched palate, low-set dysplastic ears.

E) Individual 4 at two years of age showing excessive forehead hair, arched and thick eyebrows with synophrys, epicanthus, downslanted palpebral fissures, hypertelorism,

periorbital fullness with thick eyelids, broad nasal bridge, long and smooth philtrum, wide mouth, thin upper lip, thick lower lip, low-set dysplastic ears, and webbed neck.

F) Pedigree of individual 4.

G) Individual 5 at four months showing excessive forehead hair, thick and arched eyebrows with synophrys, epicanthus, hypertelorism, periorbital fullness with thick eyelids, broad nasal bridge, thin upper lip, thick lower lip, microretrognathia, high arched palate, low-set dysplastic ears, and preauricular skin tag.

H) Pedigree of individual 5.

I) Individual 6 at four months of age showing thick and arched eyebrows with synophrys, epicanthus, hypertelorism, periorbital fullness with thick eyelids, broad and flat nasal bridge, long and smooth philtrum, wide mouth, thin upper lip, thick lower lip, low-set and dysplastic ears, and a short neck.

J) Pedigree of individual 6.

K) DeepGestalt composite image generated from facial images of individuals with genetically proven Suleiman-El-Hattab syndrome. The facial gestalt is distinct from all other descriptors of syndromes in the Face2Gene (FDNA Inc., USA) dataset (300+ syndromes).

L) *TASP1* gene structure (NM_017714.3) and corresponding protein (NP_060184.2) with respective identified variants. Please note that the missense variant p.Thr234Met has been identified in a homozygous state in case 3 in Suleiman, et al., 2019.[1]

M) Western Blot. TASP1 protein (cleaved form p28) is not observed in primary fibroblasts carrying biallelic loss-of-function variants (TASP1-Arg67*, individual 5; TASP1-trunc, individual 6) compared to primary fibroblasts from a healthy donor (405VI wt).

N) TASP1 antibody specificity was verified by downregulating *TASP1* gene expression using specific *TASP1*-targeting siRNAs. A clear reduction of TASP1 protein levels with transfection in HeLa cells was observed. NT, non-targeted siRNA; 405VI wt, primary fibroblasts of control; TASP1Arg67*, primary fibroblasts of individual 5.

Figure 2. Cranial MRI images for 4 individuals with variable degrees of posterior fossa malformations.

A) Images for individual 2 at age 8 months; sagittal T1 (A1), axial T2 (A2, A3) and coronal T2 (A4); show cystic dilatation of the fourth ventricle extending posteriorly and directly communicating with massively enlarged posterior fossa, with associated hypoplasia/dysgenesis of cerebellar vermis and small cerebellar hemispheres and cephalad rotation of the vermian remnant (Dandy-Walker malformation). In addition, significant supratentorial hydrocephalus with dilated lateral and third ventricles is seen causing stretching of the overlying corpus callosum.

B) Images for individual 3 at age 5 months; sagittal T2 (B1, B2) ,axial T2 (B3) and axial T1 (B4); show a well-defined right cerebellopontine angle cyst 1.2x1.5x1.5 cm (arrow in B2, 3, 4) and hypoplasia of the splenium of corpus callosum (best seen in B1).

C) Images for individual 5 at age 3 years; sagittal T2 (C1), axial T2 (C2, C33) and axial FLAIR (C4) show dilatation of the fourth ventricle that directly communicate with mildly enlarged posterior fossa, with associated hypoplastic inferior cerebellar vermis. In addition, dilatation of lateral and third ventricles is seen, as well as periventricular white matter hyperintensity around posterior horn of lateral ventricle bilaterally (seen best in C4).

D) Images for individual 6 at age 6 years; sagittal T1 (D1), axial T2 (D2, D3) and coronal T2 (D4) show dilatation of the fourth ventricle that directly communicate with a retrocerebellar cyst, with associated hypoplastic inferior vermis. In addition, dilatation of lateral and third ventricles is seen.

Figure 3. RNA sequencing, proteomics, and DNA methylation

A) Volcano plot showing significant outliers of RNA sequencing with notable differentially expressed genes marked.

B) Volcano plot showing significant outliers of quantitative proteomics with notable differentially expressed protein marked.

C) Principal component analysis (PCA) based on DNAm values at 114 Kabuki syndrome 1 signature sites clearly distinguishes the DNAm profile of healthy controls (n = 65 controls presented as grey dots), from DNAm profiles of the five individuals with Kabuki syndrome 1 (orange dots) on the first principal component (PC1) and the two individuals carrying *TASP1* variants (blue; individuals 4 and 5) on PC2.[17]

D) Hierarchal clustering shows that, at Kabuki syndrome 1 signature sites, individuals carrying *TASP1* variants have DNAm profiles that are intermediate when compared to the DNAm profiles of Kabuki syndrome 1 individuals and controls. Euclidean distance metric is used in the clustering dendrogram and the color gradient indicates the normalized β (DNAm) value ranging from -2.0 (blue) to +2.0 (yellow).

Figure 4

A) Sequence of EKW control larvae and a homozygous, *tasp1* larva with c.313_314delTC, predicting p.Ser105Gly*fs**2 (ENSDART00000133661.3).

B) and C) Measurement of brain area in homozygous, *tasp1* indel larvae shows a smaller size compared to wildtype control larvae. B) Measurement of brain area from control larvae at 6 days post fertilization (dpf). Larval brain area was measured from an average of 5 consecutive sections of brain containing diencephalon (red dotted line).

C) Measurement of brain area from homozygous, *tasp1* indel larvae at 6 days post fertilization (dpf). Larval brain area was measured from an average of 5 consecutive sections of brain containing diencephalon (red dotted line). This difference was not statistically significant.

D) to L) Homozygous, *tasp1* indel larvae show abnormal development and hypoplasia of the cranial cartilages at 6 days post fertilization (dpf) compared to wildtype controls. bb, basibranchial; bh, basihyal; cb, ceratobranchial; ch, ceratohyal; e, ethmoid plate; m, Meckel's cartilage; pq, palatoquadrate; t, trabeculae cranii.

D) Dorsal view of cranial cartilages in 6dpf EKW control larvae. E) Lateral view of cranial cartilages in 6dpf control larvae. F) Ventral view of cranial cartilages in 6dpf control larvae. G) Dorsal view of 6dpf *tasp1* homozygous larvae with mild abnormality in cranial cartilages, showing ethmoid plate length is slighter shorter compared to EKW control. H) Lateral view of 6dpf *tasp1* homozygous larvae with mild abnormality in cranial cartilages, showing ceratohyal length are shorter compared to EKW control. I) Ventral view of 6dpf *tasp1* homozygous larvae with mild abnormality in cranial cartilages, showing wider angle between ceratohyal compared to EKW control. J) Dorsal view of 6dpf *tasp1* homozygous larvae with severe abnormality in cranial cartilages, showing ethmoid plate

is severely shorter and trabeculae cranii is abnormally positioned by growing further toward lateral compared to EKW control. K) Lateral view of 6dpf *tasp1* homozygous larvae with severe abnormality in cranial cartilages, showing that trabeculae are abnormally positioned and appear to be more ventrally located and the ceratohyal cartilage appears to be shorter compared to EKW control. L) Ventral view of 6dpf *tasp1* homozygous larvae with severe abnormality in cranial cartilages; Ceratobranchial and ceratohyal are shorter; Basibranchial and basihyal are also shorter in length and contribute to the larger angle between ceratohyal cartilages; Palatoquadrate and Meckel appear shorter in tasp1 homozygous larvae with a phenotype and thus the lower jaw length appears shorter than the upper jaw.

Supplementary Table S1. Significant differentially expressed genes in RNA sequencing

Supplementary Table S2. Significant differentially expressed proteins in proteomics.

Data availability

Data are available upon request at the respective authors' institutions.

Acknowledgements

All authors thank the families for participating in the study.

Author Information

KMR and AWEH performed data analysis, designed the study and wrote the manuscript. ALB, JA, VC, KS, JH, and JS provided phenotypic and genotypic data. PLK, CP, SH, AMS, DA, CB, NB, ZA,RW, TM, and RK did functional and data analyses. All authors critically reviewed and revised the manuscript.

Ethics Declaration

This study was approved by the ethics committee of the Technical University of Munich, Munich, Germany and the ethics committees of the respective author's institution.

References

1. Suleiman J, Riedhammer KM, Jicinsky T, et al. Homozygous loss-of-function variants of TASP1, a gene encoding an activator of the histone methyltransferases KMT2A and KMT2D, cause a syndrome of developmental delay, happy demeanor, distinctive facial features, and congenital anomalies. Hum Mutat. 2019;40(11):1985-1992.
2. Niizuma H, Cheng EH, Hsieh JJ. Taspase 1: A protease with many biological surprises. Mol Cell Oncol. 2015;2(4):e999513.
3. Bjornsson HT. The Mendelian disorders of the epigenetic machinery. Genome Res. 2015;25(10):1473-1481.
4. Jones WD, Dafou D, McEntagart M, et al. De novo mutations in MLL cause Wiedemann-Steiner syndrome. Am J Hum Genet. 2012;91(2):358-364.
5. Zech M, Boesch S, Maier EM, et al. Haploinsufficiency of KMT2B, Encoding the Lysine-Specific Histone Methyltransferase 2B, Results in Early-Onset Generalized Dystonia. Am J Hum Genet. 2016;99(6):1377-1387.
6. Ng SB, Bigham AW, Buckingham KJ, et al. Exome sequencing identifies MLL2 mutations as a cause of Kabuki syndrome. Nat Genet. 2010;42(9):790-793.
7. Sobreira N, Schiettecatte F, Valle D, Hamosh A. GeneMatcher: a matching tool for connecting investigators with an interest in the same gene. Hum Mutat. 2015;36(10):928-930.
8. Gambin T, Yuan B, Bi W, et al. Identification of novel candidate disease genes from de novo exonic copy number variants. Genome Med. 2017;9(1):83.
9. Alabdullatif MA, Al Dhaibani MA, Khassawneh MY, El-Hattab AW. Chromosomal microarray in a highly consanguineous population: diagnostic yield, utility of regions of homozygosity, and novel mutations. Clin Genet. 2017;91(4):616-622.
10. Kremer LS, Bader DM, Mertes C, et al. Genetic diagnosis of Mendelian disorders via RNA sequencing. Nat Commun. 2017;8:15824.
11. Riedhammer KM, Stockler S, Ploski R, et al. De novo stop-loss variants in CLDN11 cause hypomyelinating leukodystrophy. Brain. 2021;144(2):411-419.
12. Ucuncu E, Rajamani K, Wilson MSC, et al. MINPP1 prevents intracellular accumulation of the chelator inositol hexakisphosphate and is mutated in Pontocerebellar Hypoplasia. Nat Commun. 2020;11(1):6087.
13. Gurovich Y, Hanani Y, Bar O, et al. Identifying facial phenotypes of genetic disorders using deep learning. Nat Med. 2019;25(1):60-64.
14. Despras E, Sittewelle M, Pouvelle C, Delrieu N, Cordonnier AM, Kannouche PL. Rad18-dependent SUMOylation of human specialized DNA polymerase eta is required to prevent under-replicated DNA. Nat Commun. 2016;7:13326.

15. Brechtmann F, Mertes C, Matuseviciute A, et al. OUTRIDER: A Statistical Method for Detecting Aberrantly Expressed Genes in RNA Sequencing Data. Am J Hum Genet. 2018;103(6):907-917.
16. Choufani S, Cytrynbaum C, Chung BH, et al. NSD1 mutations generate a genome-wide DNA methylation signature. Nat Commun. 2015;6:10207.
17. Butcher DT, Cytrynbaum C, Turinsky AL, et al. CHARGE and Kabuki Syndromes: Gene-Specific DNA Methylation Signatures Identify Epigenetic Mechanisms Linking These Clinically Overlapping Conditions. Am J Hum Genet. 2017;100(5):773-788.
18. Wu D, Mandal S, Choi A, et al. DLX4 is associated with orofacial clefting and abnormal jaw development. Hum Mol Genet. 2015;24(15):4340-4352.
19. Takeda S, Sasagawa S, Oyama T, et al. Taspase1-dependent TFIIA cleavage coordinates head morphogenesis by limiting Cdkn2a locus transcription. J Clin Invest. 2015;125(3):1203-1214.
20. Kollias SS, Ball WS, Jr., Prenger EC. Cystic malformations of the posterior fossa: differential diagnosis clarified through embryologic analysis. Radiographics. 1993;13(6):1211-1231.
21. Barkovich AJ, Kjos BO, Norman D, Edwards MS. Revised classification of posterior fossa cysts and cystlike malformations based on the results of multiplanar MR imaging. AJR Am J Roentgenol. 1989;153(6):1289-1300.
22. Aldinger KA, Timms AE, Thomson Z, et al. Redefining the Etiologic Landscape of Cerebellar Malformations. Am J Hum Genet. 2019;105(3):606-615.
23. Hsieh JJ, Cheng EH, Korsmeyer SJ. Taspase1: a threonine aspartase required for cleavage of MLL and proper HOX gene expression. Cell. 2003;115(3):293-303.
24. Takeda S, Chen DY, Westergard TD, et al. Proteolysis of MLL family proteins is essential for taspase1-orchestrated cell cycle progression. Genes Dev. 2006;20(17):2397-2409.
25. Zhou H, Spicuglia S, Hsieh JJ, et al. Uncleaved TFIIA is a substrate for taspase 1 and active in transcription. Mol Cell Biol. 2006;26(7):2728-2735.
26. Meyer E, Carss KJ, Rankin J, et al. Mutations in the histone methyltransferase gene KMT2B cause complex early-onset dystonia. Nat Genet. 2017;49(2):223-237.
27. Shilatifard A. The COMPASS family of histone H3K4 methylases: mechanisms of regulation in development and disease pathogenesis. Annu Rev Biochem. 2012;81:65-95.
28. Aref-Eshghi E, Kerkhof J, Pedro VP, et al. Evaluation of DNA Methylation Episignatures for Diagnosis and Phenotype Correlations in 42 Mendelian Neurodevelopmental Disorders. Am J Hum Genet. 2020;106(3):356-370.
29. Van Laarhoven PM, Neitzel LR, Quintana AM, et al. Kabuki syndrome genes KMT2D and KDM6A: functional analyses demonstrate critical roles in craniofacial, heart and brain development. Hum Mol Genet. 2015;24(15):4443-4453.

Conflict of interest

The authors declare no conflict of interest.

Table 1. Genotypic and phenotypic characteristics of individuals with Suleiman-El-Hattab syndrome

Will be deleted	**Saeed**	**Salem**	**Mahra**	**Dana**	**Germany**	**France**		
Individual	**1**	**2**	**3**	**4**	**5**	**6**	**Case 3[a]**	
Gender	Male	Male	Female	Female	Male	Female	Male	
Ethnicity	Arabian Peninsula	Arabian Peninsula	Arabian Peninsula	Arabian Peninsula	Turkish	North Africa	Arabian Peninsula	
Age	7 years	9 months	19 months	3 years	6 years	10 years	3 years	
***TASP1* allele 1**	Exon 5 – 11 deletion	Exon 5 – 11 deletion	Exon 5 – 11 deletion	Exon 5 – 11 deletion	c.199C>T p.(Arg67*)	c.81del p.(Glu29Serfs*79)	c.701C>T p.(Thr234Met)	
***TASP1* allele 2**	Exon 5 – 11 deletion	Exon 5 – 11 deletion	Exon 5 – 11 deletion	Exon 5 – 11 deletion	c.199C>T p.(Arg67*)	c.(598_599del) p.(Lys200Glufs*24)	c.701C>T p.(Thr234Met)	
Neurodevelopment								
Developmental delay	+	+	+	+	+	+	+	**7/7**
Hypotonia	+	+	+	+	+	-	+	**6/7**
Microcephaly	+	-	+	+	+	+	+	**6/7**
Seizures	-	-	-	-	+	-	+	**2/7**
Posterior fossa malformation	-	+	+	-	+	+	-	**4/7**
Dilated ventricles	-	+	-	-	+	+	+	**4/7**
Feeding and growth								
Feeing difficulties	+	+	+	+	+	+	+	**7/7**
Salivary drooling	+	-	+	+	-	-	+	**4/7**
Failure to thrive	+	+	+	+	-	-	+	**5/7**
Happy demeanor	+	**NA (too young)**	+	+	+	-	+	**5/6**
CVS malformation	ASD/VSD	TOF	PFO/VSD	PFO/VSD	VSD	VSD	-	**6/7**
Cryptorchidism	+	-	**NA**	**NA**	+	**NA**	+	**3/4**
Hirsutism	+	-	+	+	-	+	-	**4/7**
Rec resp infections	+	-	+	+	+	-	-	**4/7**
Preauricular skin tag	-	+	+	+	+	-	-	**4/7**
Single palmar crease	+	-	-	+	+	-	-	**3/7**
Facial features								
Prominent glabella	+	+	+	-			+	**4/7**
Excess forehead hair	+	-	+	+	+	-	-	**4/7**
Thick eyebrows	+	+	+	+	+	+	+	**7/7**
Arched eyebrows	+	+	+	+	+	+	+	**7/7**
Synophrys	+	+	+	+	+	+	+	**7/7**
Epicanthus	+	+	+	+	+	+	+	**7/7**
Hypertelorism	+	+	+	+	+	+	+	**7/7**

Downslanted eyes	-	-	+	+	-	-	-	2/7
Thick eyelids	+	+	+	+	+	+	+	7/7
Periorbital fullness	+	+	+	+	+	+	+	7/7
Broad nasal bridge	+	+	+	+	+	+	+	7/7
Long smooth philtrum	+	+	+	+	-	+	+	6/7
Wide mouth	+	+	+	+	-	+	+	6/7
Thin upper lip	+	+	+	+	+	+	+	7/7
Thick lower lip	+	+	+	+	+	+	+	7/7
Microretrognathia	-	+	+	-	+	-	-	3/7
High arched palate	-	-	+	-	+	-	-	2/7
Low-set ears	+	+	+	+	+	+	+	7/7
Dysplastic ears	+	+	+	+	+	+	+	7/7
Webbed neck	+	-	+	+	-	-	-	3/7
Ophthalmologic anomalies				Hyperopia	Strabismus, amblyopia, pale optic disc	Hyperopia		
Limb deformities	Brachydactyly, clinodactyly	Overlapping toes		Polydactyly		Short extremities, brachydactyly, broad thumb and first toe		
Skeletal deformities						Scoliosis, genu recurvatum	Short stature	
Skin	-	Lumbar skin dimple	Sacral hair tuft,	Congenital dermal melanocytosis	-	-	-	
Others	Hearing impairment	-	Umbilical hernia	Left hydronephrosis	Inguinal hernia	Choanal stenosis, anteriorly placed anus, spasticity of the lower limbs	-	

ASD, atrial septal defect; CNS, central nervous system; CSF, cerebrospinal fluid; NA, not applicable; PFO, patent foramen ovale; TOF, tetralogy of Fallot; VSD, ventricular septal defect. *TASP1* transcript NM_017714.3, TASP1 protein NP_060184.2.
[a]Described in [1], no new phenotypic or functional data. Featured in the table and the discussion to present all reported individuals with Suleiman-El-Hattab syndrome.

1. Suleiman J, Riedhammer KM, Jicinsky T, et al. Homozygous loss-of-function variants of TASP1, a gene encoding an activator of the histone methyltransferases KMT2A and KMT2D, cause a syndrome of developmental delay, happy demeanor, distinctive facial features, and congenital anomalies. Hum Mutat. 2019;40(11):1985-1992.


A


B


E


G


I


K

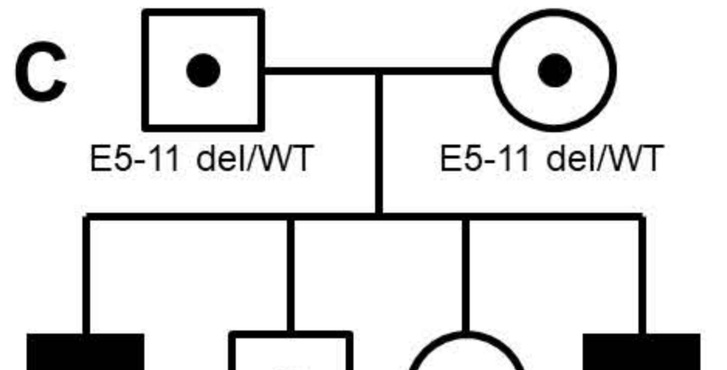
C
E5-11 del/WT
E5-11 del/WT
E5-11 del/ E5-11 del
E5-11 del/ WT
WT/WT
E5-11 del/ E5-11 del

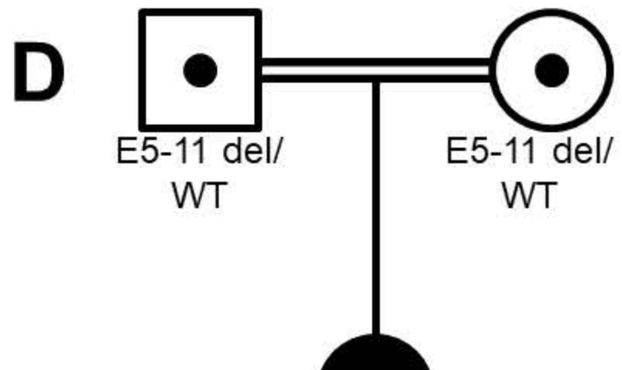
D
E5-11 del/ WT
E5-11 del/ WT
E5-11 del/ E5-11 del

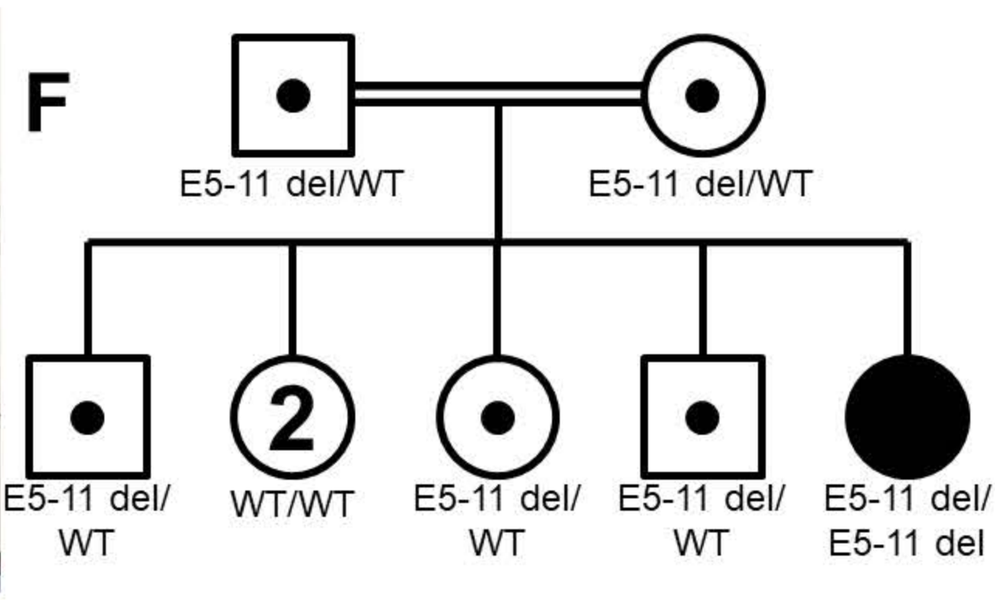
F
E5-11 del/WT
E5-11 del/WT
E5-11 del/ WT
2
WT/WT
E5-11 del/ WT
E5-11 del/ WT
E5-11 del/ E5-11 del

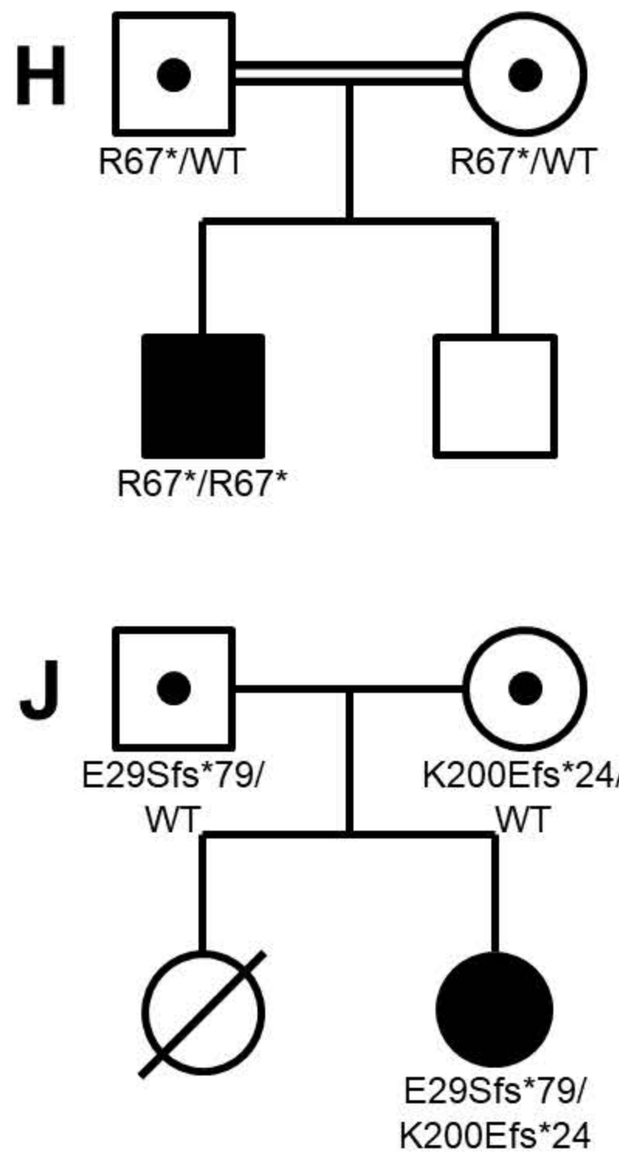
H
R67*/WT
R67*/WT
R67*/R67*
J
E29Sfs*79/ WT
K200Efs*24/ WT
E29Sfs*79/ K200Efs*24

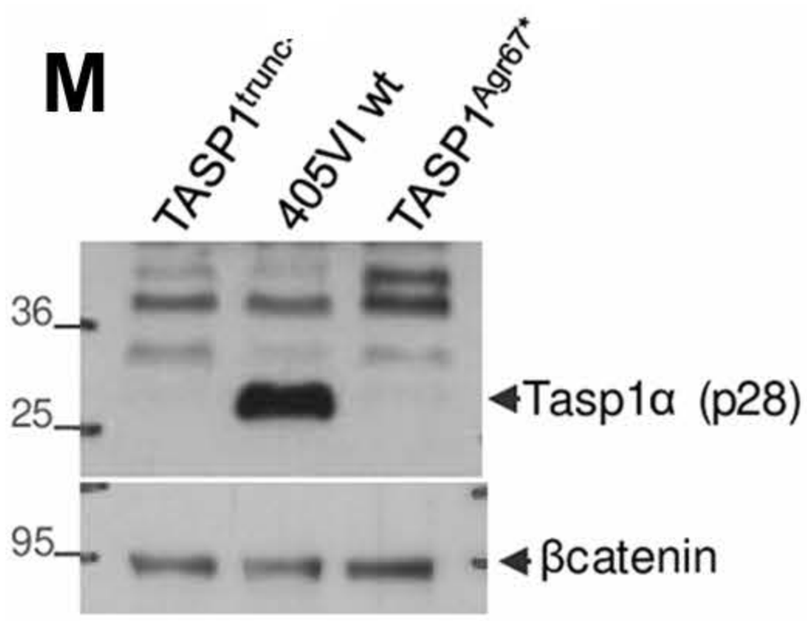
M
TASP1trunc.
405V/I wt
TASP1Agr67*
36
25
Tasp1α (p28)
95
βcatenin

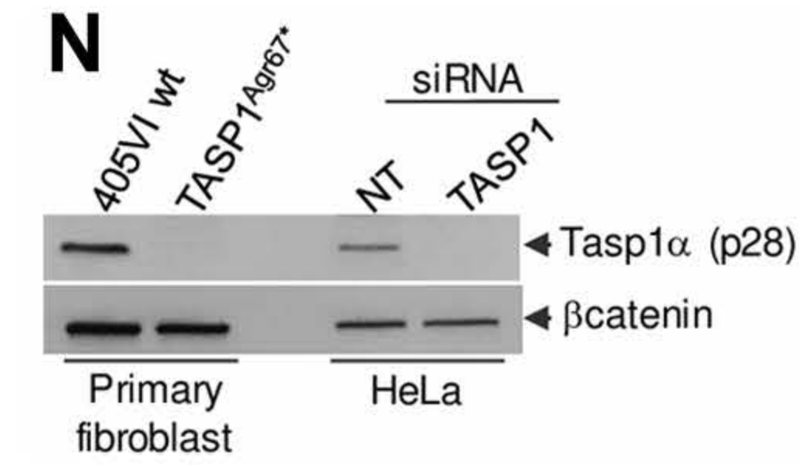
N
405V/I wt
TASP1Agr67*
siRNA
NT
TASP1
Tasp1α (p28)
βcatenin
Primary fibroblast
HeLa

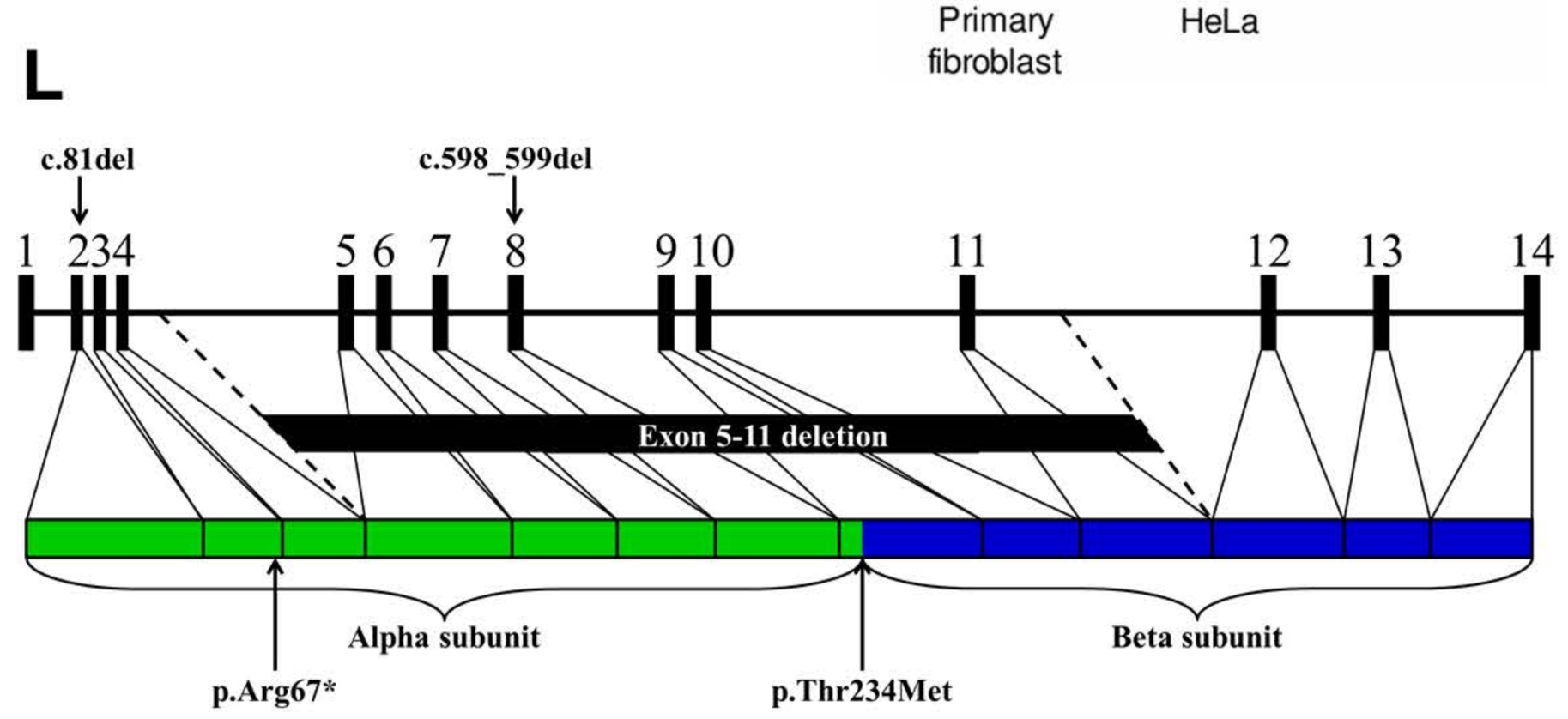
L
c.81del
c.598_599del
1 234 5 6 7 8 9 10 11 12 13 14
Exon 5-11 deletion
Alpha subunit
Beta subunit
p.Arg67*
p.Thr234Met

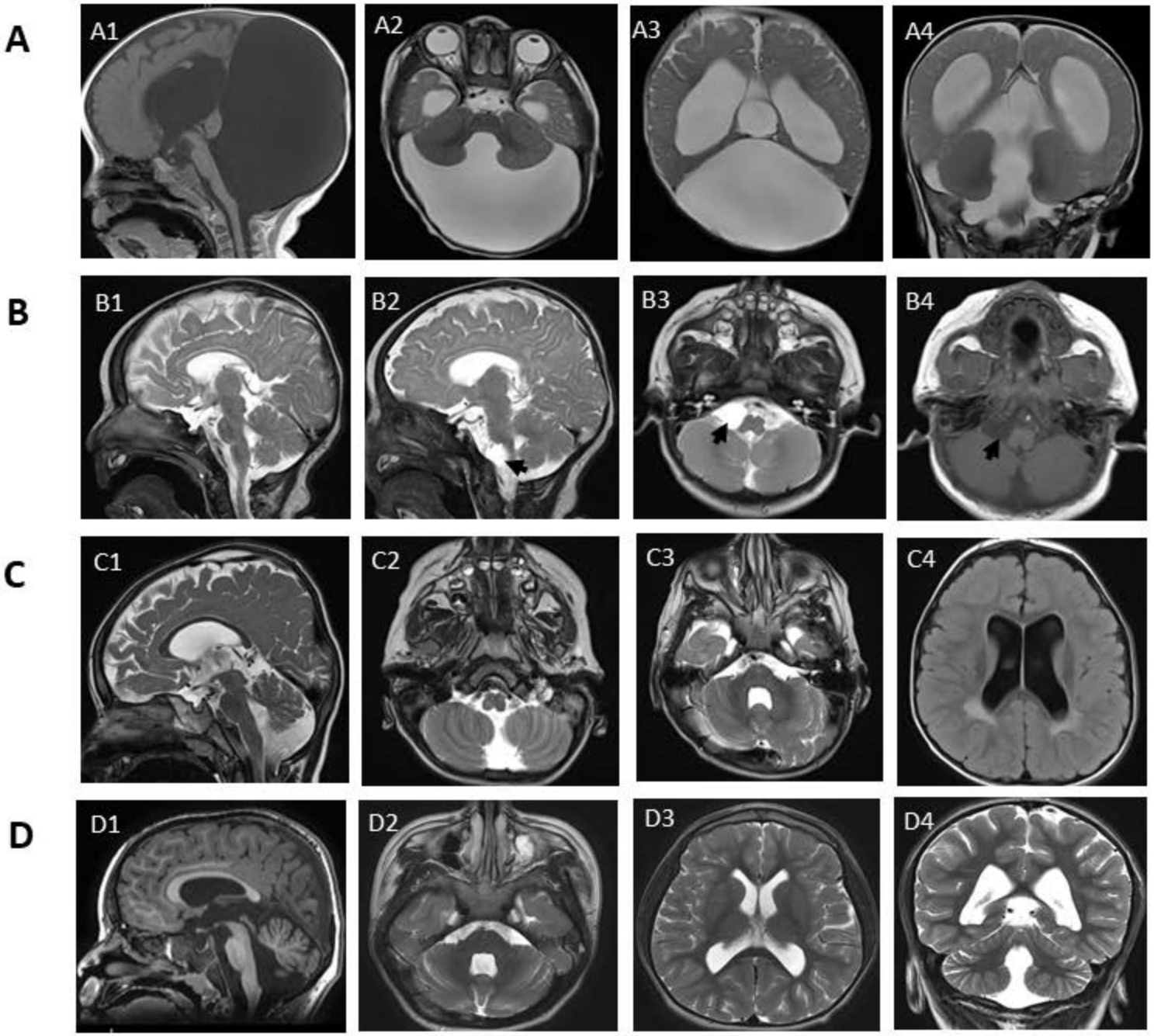
A
A1
A2
A3
A4
B
B1
B2
B3
B4
C
C1
C2
C3
C4
D
D1
D2
D3
D4

A

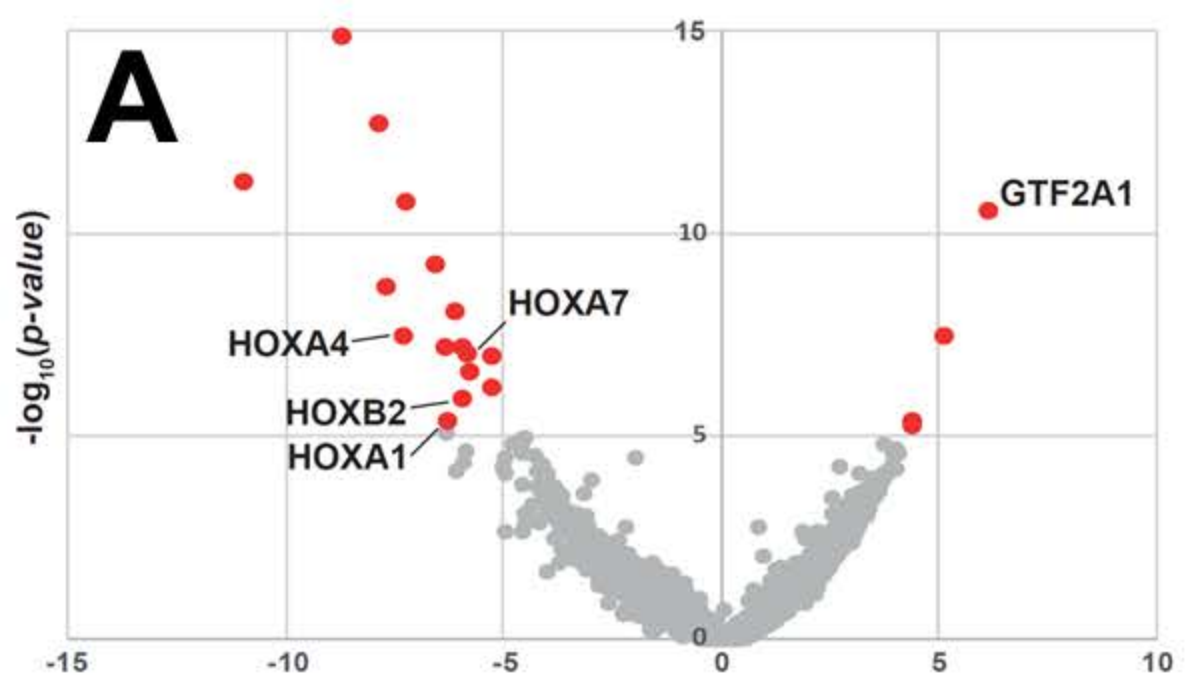
-log10(p-value)
15
10
5
0
-15
-10
-5
0
5
10
GTF2A1
HOXA7
HOXA4
HOXB2
HOXA1

B

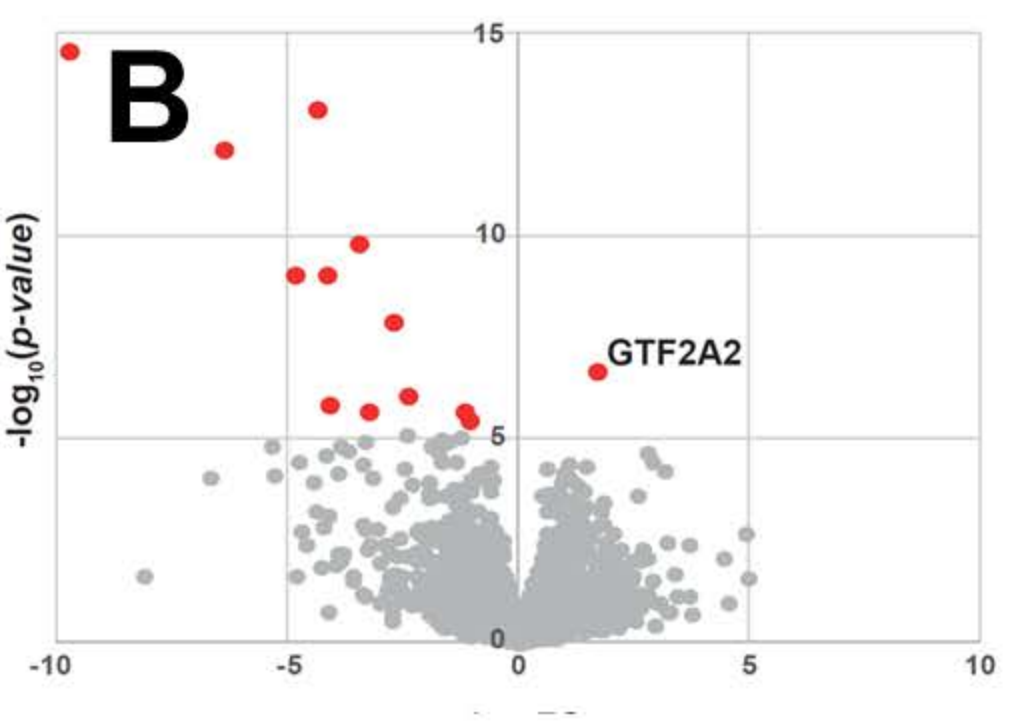
-log10(p-value)
15
10
5
0
-10
-5
0
5
10
GTF2A2

C

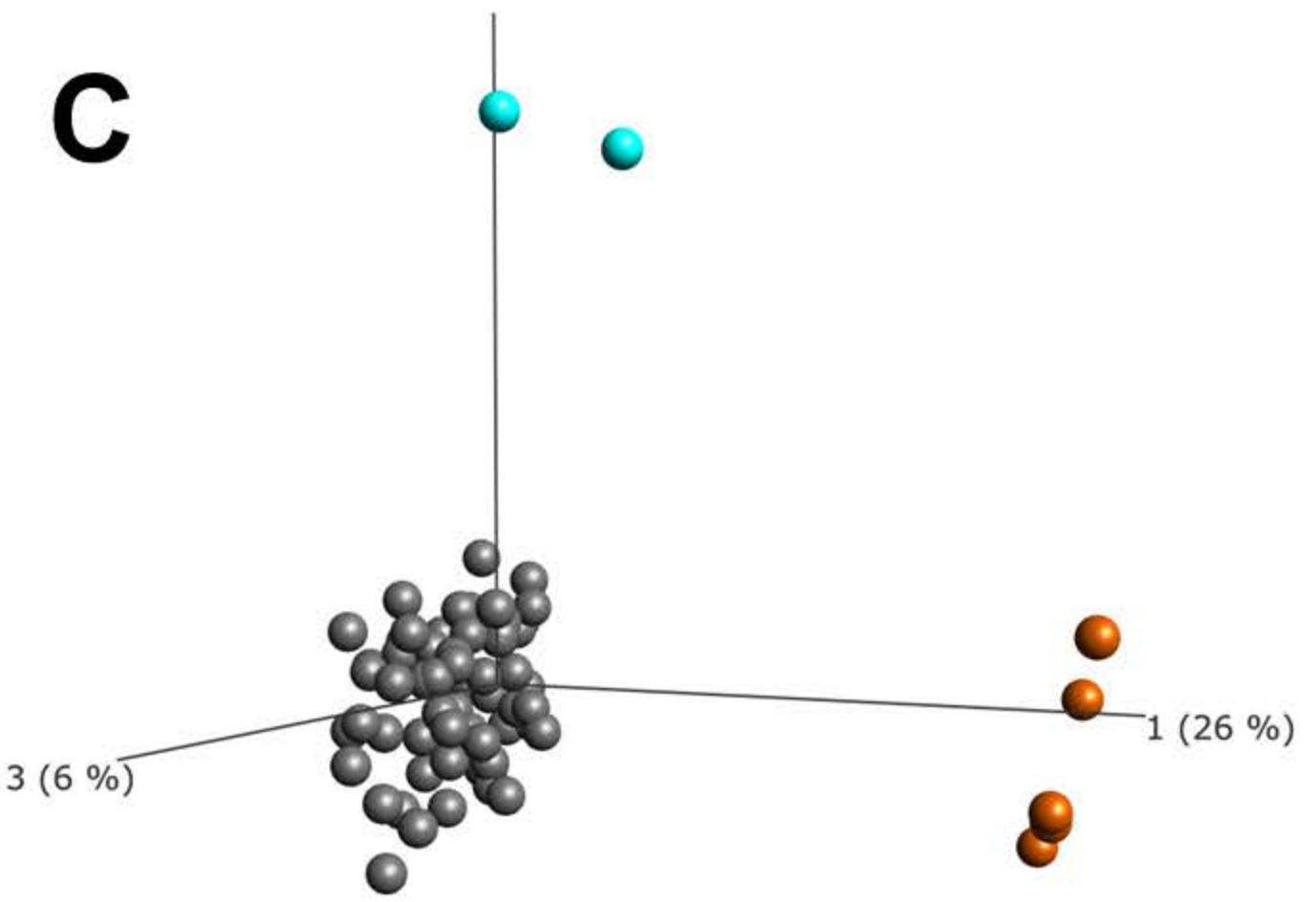
2 (12 %)
1 (26 %)
3 (6 %)

D

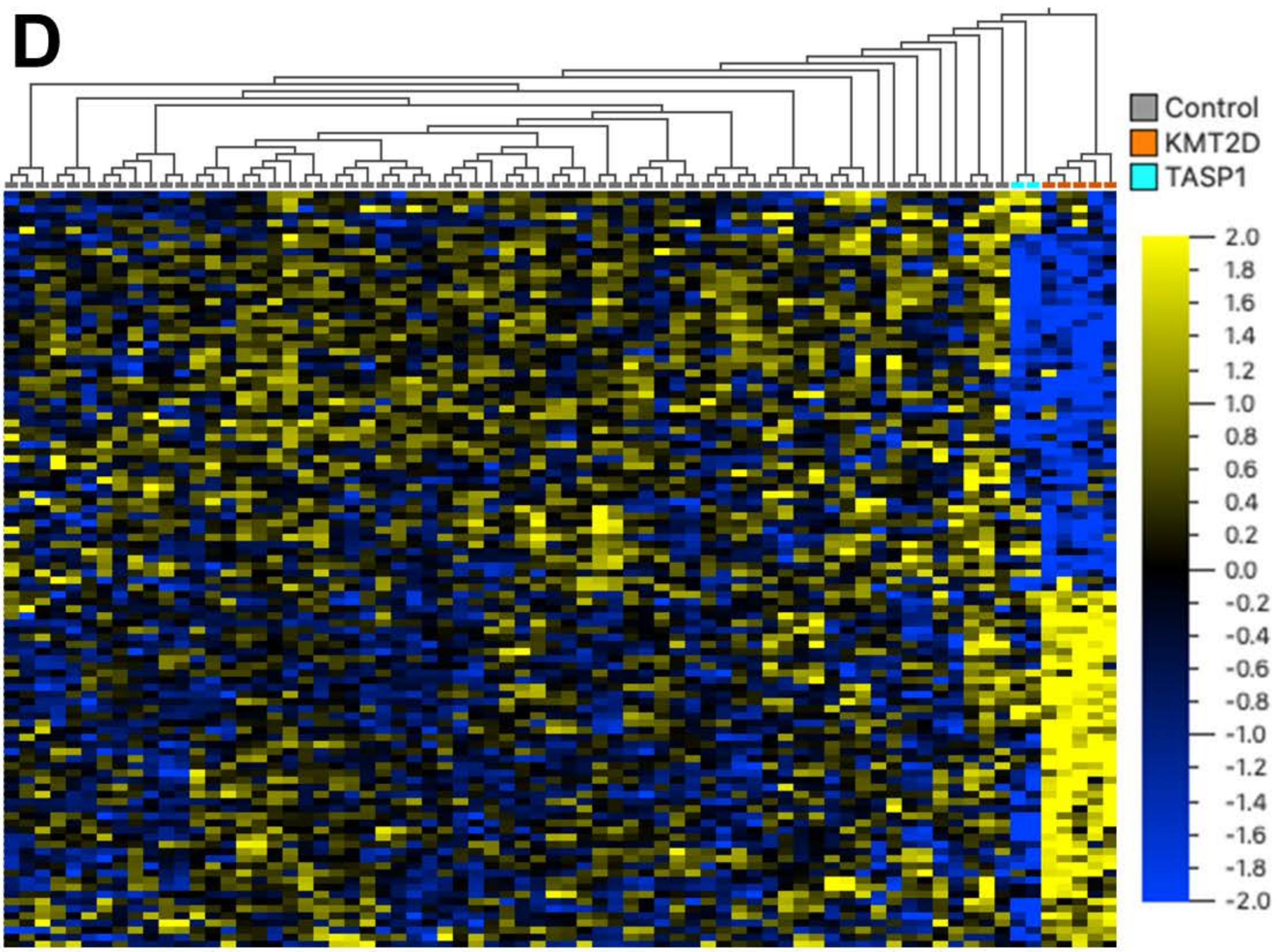
Control
KMT2D
TASP1
2.0
1.8
1.6
1.4
1.2
1.0
0.8
0.6
0.4
0.2
0.0
-0.2
-0.4
-0.6
-0.8
-1.0
-1.2
-1.4
-1.6
-1.8
-2.0

A

EKW control

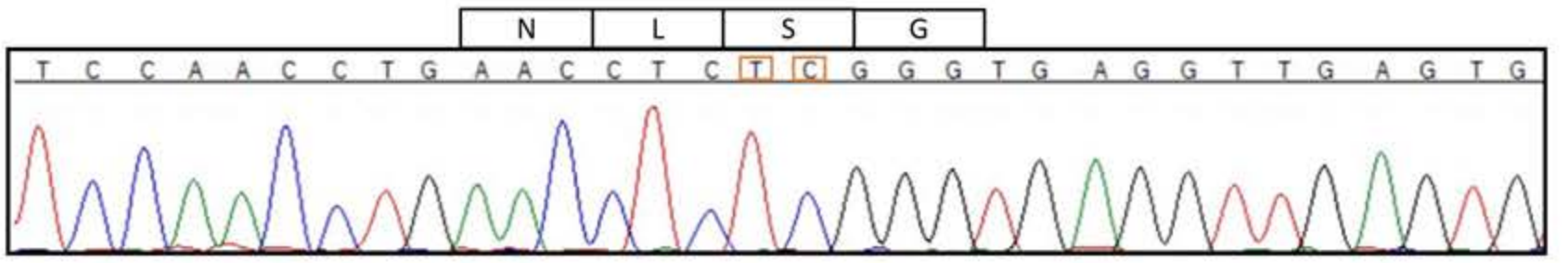

tasp1
c.313_314delTC:
p.Ser105Glyfs*2

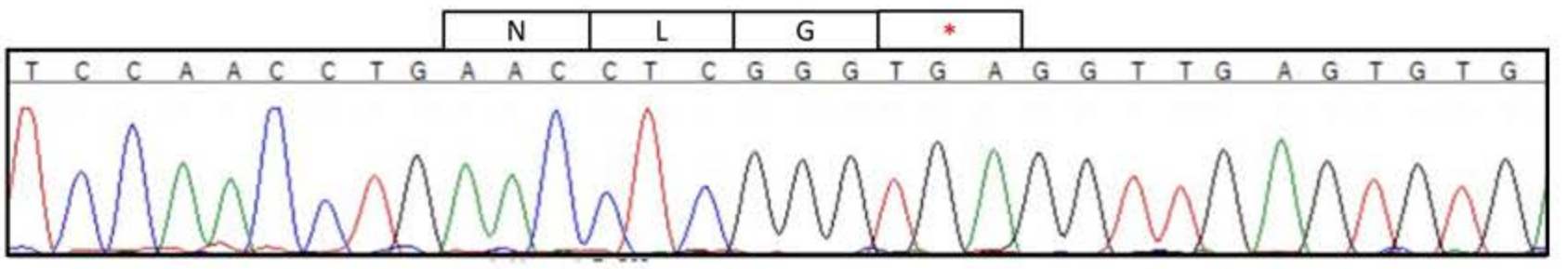

B

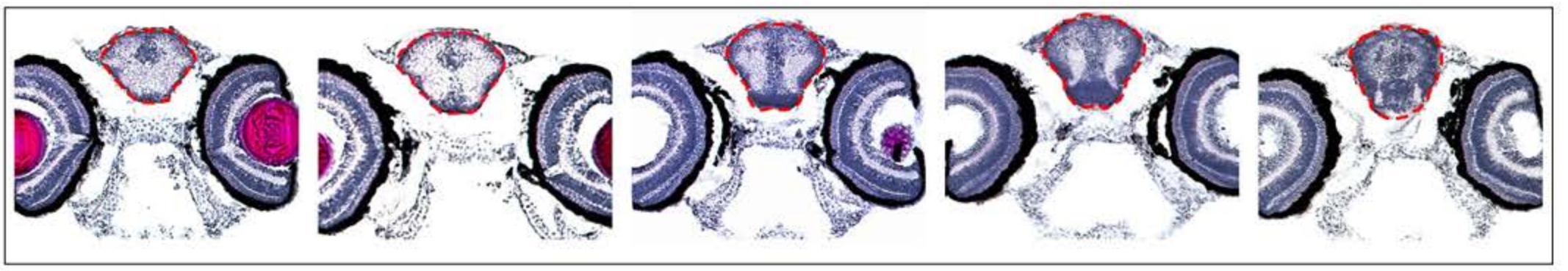

C

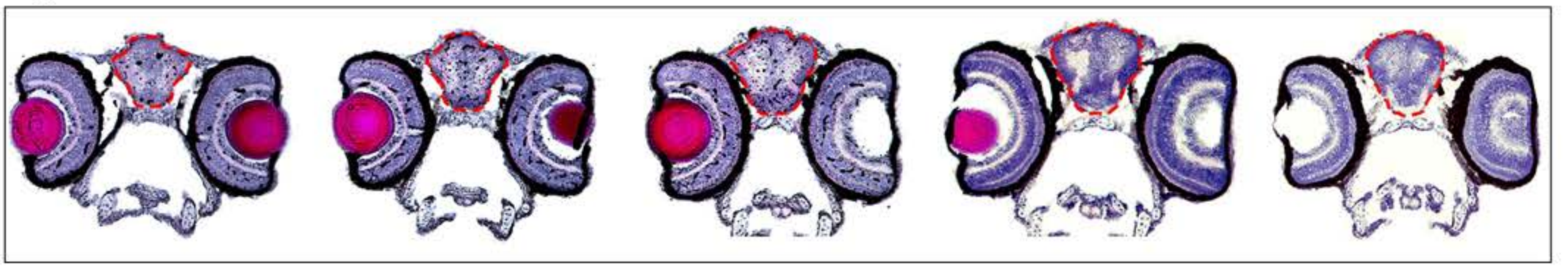

Dorsal Lateral Ventral

EKW Control

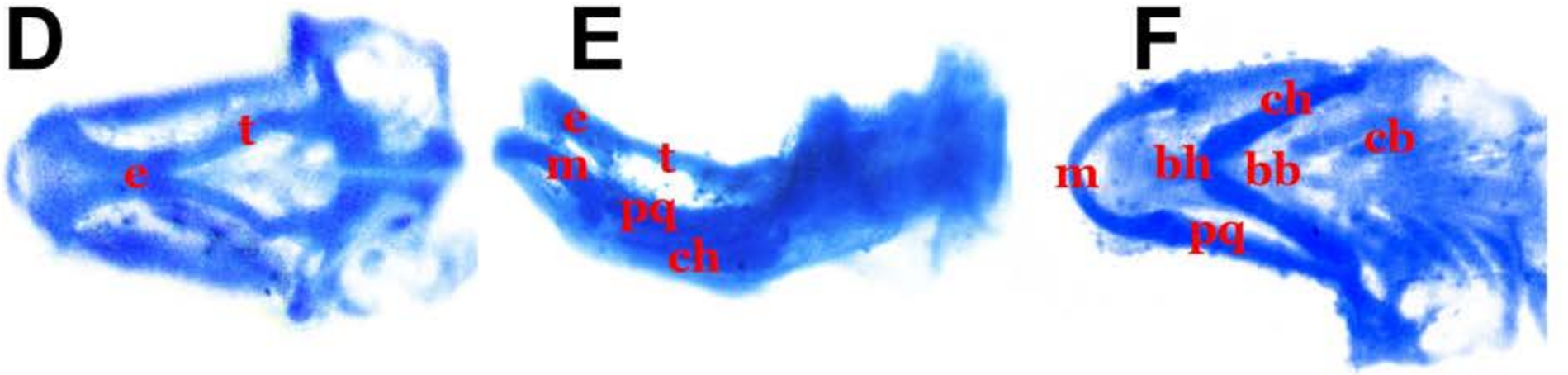

tasp1 indel homozygote

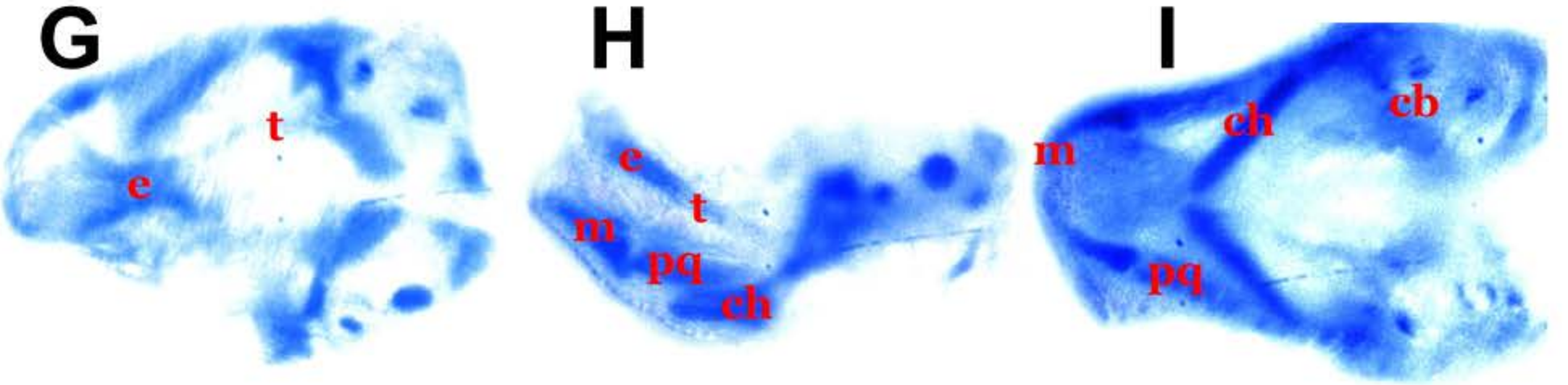

tasp1 indel homozygote

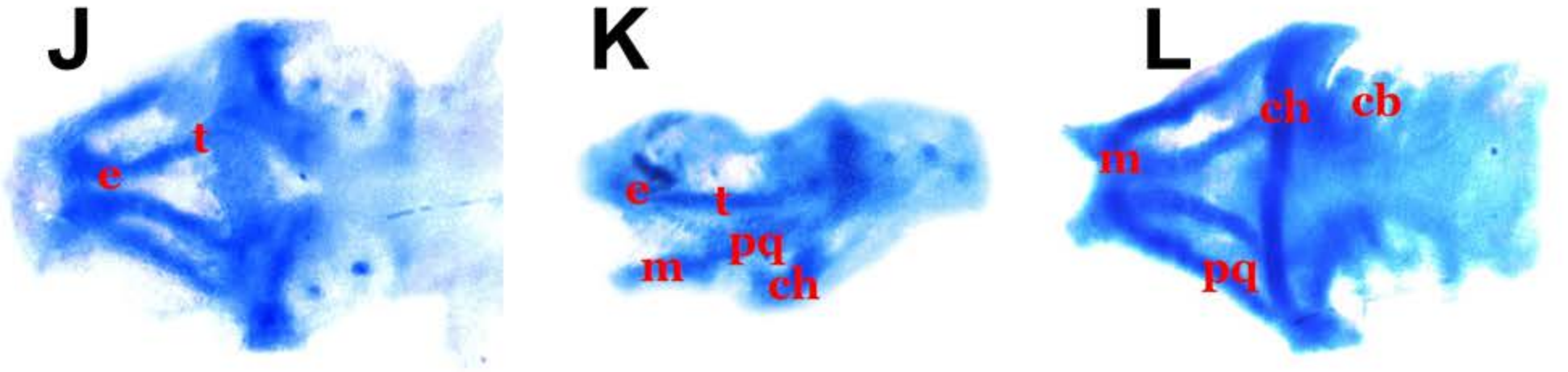

geneID	pValue	padjust	zScore	l2fc	rawcounts	normcounts
PIGG	1,42E-15	2,03E-10	-8,72	-0,95	850	998,68
ERLEC1	1,96E-13	1,40E-08	-7,88	-0,65	2053	2540,4
NRN1	5,50E-12	2,62E-07	-11	-9,63	0	0
LGALS1	1,58E-11	5,63E-07	-7,27	-0,99	19034	14640,58
GTF2A1	2,86E-11	8,15E-07	6,12	0,55	4922	2894,86
TPT1	5,64E-10	1,34E-05	-6,55	-0,64	33894	36164,8
HECW2	2,15E-09	4,39E-05	-7,71	-3,1	45	66,46
AHCY	8,12E-09	0,00014485	-6,13	-0,62	2357	2685,59
TCEAL1	3,25E-08	0,00050231	5,14	0,62	765	762,13
HOXA4	3,52E-08	0,00050231	-7,33	-5,42	0	0
AC099522.1_2	6,57E-08	0,0007864	-6,34	-1,57	495	592,73
HOXA7	6,61E-08	0,0007864	-5,98	-5,4	3	4
MRPL48	1,00E-07	0,00103773	-5,86	-0,7	358	407,15
FOXD1	1,02E-07	0,00103773	-5,28	-1,54	525	690,18
TSPAN31	2,45E-07	0,00233172	-5,78	-0,77	391	717,7
ZDHHC13	6,43E-07	0,00573833	-5,25	-0,73	399	341,78
HOXB2	1,13E-06	0,00950172	-5,93	-1,8	59	163,35
SSR4	4,10E-06	0,03120586	4,37	0,44	4677	4526,23
HOXA1	4,16E-06	0,03120586	-6,32	-5,15	0	0
TCEAL4	5,33E-06	0,03804319	4,39	0,38	3402	4355,32

meanCorrected	FC
1936,18	0,5176
3976,55	0,6373
3368,73	0,0013
29022,65	0,5035
1971,87	1,4641
56298,36	0,6417
580,36	0,1166
4129,95	0,6507
495,66	1,5369
73,16	0,0234
1685,19	0,3368
224,19	0,0237
661,32	0,6156
2023,47	0,3439
1224,9	0,5864
566,65	0,6029
576,19	0,2872
3327,68	1,3566
64,28	0,0282
3347,26	1,3013

UNIPROT_ID	NORM_LOG2_LFQ	PROT_LOG2FC	PROT_PVALUE	PROT_PADJ	GENE_NAME	SD_NORM_LOG2_LFQ
Q9NPD7	7,365336173	-9,75386215	2,9942E-15	2,3223E-11	NRN1	1,52347471
Q9Y605	12,95248602	-4,33719768	7,5524E-14	5,8569E-10	MRFAP1	0,66004445
O95873	8,162463745	-6,37832631	7,9015E-13	6,1269E-09	C6orf47	1,04723027
Q5TH69	12,33725394	-3,42731265	1,5143E-10	1,1741E-06	ARFGEF3	0,77510661
Q9NZJ9	12,01234424	-4,82755258	9,4503E-10	7,3259E-06	NUDT4	0,90094698
Q49AR2	12,03486474	-4,1287033	9,7016E-10	7,5197E-06	C5orf22	0,72885717
Q7Z4G4	14,97618142	-2,69079575	1,3991E-08	0,00010843	TRMT11	0,50288037
P52657	21,03845828	1,74251588	2,2842E-07	0,00177006	GTF2A2	0,35159684
Q9P0W2	12,67099922	-2,36640106	9,4495E-07	0,00732149	HMG20B	0,52268973
Q15389	9,970061372	-4,07331063	1,4991E-06	0,01161331	ANGPT1	0,90278655
Q9Y3E2	13,83854973	-3,24625178	2,0674E-06	0,0160137	BOLA1	0,71380009
P09382	25,54150264	-1,16057451	2,2703E-06	0,01758372	LGALS1	0,2525963
Q86SZ2	19,15857347	-1,0678533	3,6667E-06	0,02839496	TRAPPC6B	0,23651313

PROT_ZSCORE	signif	FC
-6,40237878	TRUE	0,00115823
-6,5710691	TRUE	0,049473587
-6,09066268	TRUE	0,012020775
-4,42173064	TRUE	0,092955713
-5,35830929	TRUE	0,035217771
-5,66462606	TRUE	0,057165823
-5,35076713	TRUE	0,154878013
4,95600556	TRUE	3,346181913
-4,52735324	TRUE	0,193928795
-4,51193102	TRUE	0,059403402
-4,54784446	TRUE	0,105385495
-4,59458236	TRUE	0,447334361
-4,51498524	TRUE	0,47702828